A Physical Approach to Infrared Image Understanding

C. Caillas
Centre de Recherches et d'Etudes d'Arcueil
Laboratoire Système de Perception
16, bis avenue Prieur de la Côte d'Or, 94114 Arcueil, FRANCE
ccaillas@etca.fr

Abstract

In this article, we present how it is possible to recover physical parameters of objects such as reflectivity, emissivity and thermal inertia from the analysis of infrared images in outdoor scenes. Our approach is based on the extensive use of the physical laws that are at the origin of the formation of images. First, we derive a physical model that describes how surface patches of objects appear in infrared images. Second, in order to calculate the physical properties of objects, we inverse this model by using a least square fitting method. Because of the non-linearity of the model, we show that it is difficult to obtain accurate results about the physical properties. To overcome this limitation, we demonstrate that, under several assumptions, there exist some physical invariants that are more reliable than physical parameters.

1 Introduction

In order to establish descriptions of the physical world from images, some researchers exploit the fact that the intensity in the image is produced by some physical process that can be modeled. These process based on physical laws depend on many factors such as object properties, sensor parameters, illumination conditions and coefficient of transmission between the object and the sensor. Theories and algorithms using always more rigorous knowledge of the physical phenomena underlying the formation of the images have been developed [5].

Horn and Woodham pionneered work in photometric stereo, that uses a lambertian reflection model, to recover surface albedo and shape [3, 12]. More recently, models of reflection that are able to deal with more and more kinds of surface have been developed [7]. Color and highlights have been analyzed in order to segment color images [6].

While most work in physics based vision deals with intensity or color images, we chose here to explore infrared vision. Our goal is to recover physical properties of objects from infrared images. Unlike classical images, the physical process leading to the formation of infrared images involves not only reflectivity but also emissivity and thermal inertia of objects. Emissivity is defined as the ratio between the emitted radiation from a real surface and the emitted radiation from a blackbody surface at the same temperature [11]. Thermal inertia characterizes the capacity of a material to absorb and restitute the energy more or less rapidly.

In Section 2, we present a complete physical modeling, based on heat transfer physics, that allows us to understand and to predict how points of objects will appear in infrared images. In Section 3, we develop a method in order to inverse our direct physical model

BMVC 1994 doi:10.5244/C.8.21

and to recover the three physical parameters of objects (reflectivity, emissivity and thermal inertia). Applying this method to an experimental scene constituted of horizontal surfaces of sand lead to reasonable results. Although reasonable, these results come from the resolution of a typically ill-posed problem which is the backward problem for the heat equation [1]. Even if the errors on temperature are close to 0, the errors on physical properties are not necessarily close to 0. In Section 5, we evaluate the degree of ill posedness of our problem and we show the existence of three "physical invariants" that are the combinations of emissivity, reflectivity and thermal inertia. For different vectors of the three physical parameters, these invariants have the remarkable property to lead to the same temperature at the surface of objects. These invariants then define class of objects that can be distinguished. Noise effect is also studied showing that "physical invariants" are more reliable than physical parameters.

2 Physical Modeling

2.1 The Camera Equation

The pixel intensity in an infrared image is proportional to the quantity of thermal energy, lying in the infrared spectrum and coming from the corresponding point in the 3D scene. More precisely, this energy called G_{cam} is composed of two different terms: radiation emitted by the object E_{rad}, and radiation coming from the environment that is reflected by the object in the infrared spectrum $E_{r_{ir}}$. Thus, this leads to what we call the camera equation:

$$G_{cam} = E_{rad} + E_{r_{ir}} \tag{1}$$

G_{cam} is the information in the image that will allow us in Section 3 to recover the physical properties of the surface of the object. Unfortunately, the determination of the origin of G_{cam} is not possible if we only know intensity pixel. This comes from the extreme complexity of heat echange phenomena (a priori not known) that lead to G_{cam}, through the two terms E_{rad} and $E_{r_{ir}}$. In particular, E_{rad} is directly related to the temperature of the surface by the well known Stephan-Boltzmann law $E_{rad} = \epsilon\sigma T^4$ (where ϵ is the emissivity of the surface and σ is the Stephan constant). This last equation means that there is no way to model G_{cam} as a function of the physical properties of objects if the temperature at the surface of materials has not been modeled before. In the two following sections, we therefore concentrate on developing a complete modeling of the temperature at the surface of objects.

2.2 Modeling Body and Heat Exchanges

We model the body as an homogeneous semi-infinite body whose surface is planar and horizontal. The assumption of body homogeneity allows us to consider that the conductivity k, the density ρ_m and the specific heat c_p are the same everywhere in the material. Since the body is supposed to be semi-infinite with a planar surface, we can consider that the heat flux is one-dimensional and propagates along the perpendicular direction x to the surface (Figure 1). In practice, a body can be considered as a semi-infinite body if its dimensions are sufficiently large (i.e., higher than a critical dimension that depends on the physical characteristics of the material) [1].

Heat exchanges between the body and its environment are governed by the conservation law of energy which tells us that the energy received by the surface is equal to the

[1] For materials such as sand used in our experiment, the critical dimension is a few ten centimeters.

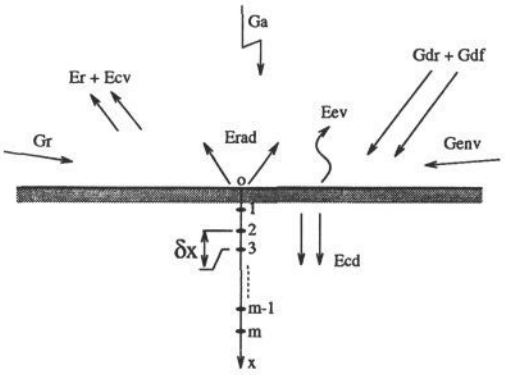

Figure 1: Heat exchanges at the surface of the body.

energy leaving the surface: $G = E$ where:

$$\begin{cases} G = G_{dr} + G_{df} + G_a + G_r + G_{env} \\ E = E_r + E_{rad} + E_{cd} + E_{cv} + E_{ev} \end{cases} \quad (2)$$

- G_{dr} is the energy coming from the sun,
- G_{df} is the diffuse energy coming from the sky,
- G_a is the energy emitted by the sky,
- G_r is the energy reflected by the environment:
- G_{env} is the energy emitted by the environment,
- E_r is the energy reflected by the surface of the object:
  1. $E_{r_{vis}}$ is the energy reflected in the visible,
  2. $E_{r_{ir}}$ is the energy reflected in the infrared,
- E_{rad} is the energy emitted by the surface of the object,
- E_{cd} is the energy conducted through the material,
- E_{cv} is the energy convected by the atmosphere,
- E_{ev} is the energy needed for water evaporation.

System 2 shows the various origins of heat exchanges between the object and its environment. These exchanges all contribute to the formation of the infrared image (Figure 1). In order to calculate the temperature of the surface, we need to explicit each term of system 2 as a function of elementary parameters.

First, direct energy G_{dr} from the sun mainly lies in the visible spectrum. In the experiment described in Section 4, this energy, falling on an horizontal surface is measured with a pyranometer placed horizontally. Diffuse energy G_{df} coming from the sky is also measured with the pyranometer. This energy comes from the diffusion of light by aerosols in all directions. Second, the emitted energy from the atmosphere G_a, lies in the infrared spectrum. In our modeling, G_a falling on an horizontal plane is not measured but approximated by using a semi-empirical equation due to Idso and Jackson [4]: $G_a = \epsilon_a \sigma T_a^4$ where T_a is the atmosphere temperature and ϵ_a is its emissivity that depends on T_a that is measured with a meteorological sensor. Third, for simplicity, we will consider that the world around the scene, seen by the camera, is flat and horizontal. Then, the energy reflected by the environment and falling on the horizontal surface of the

object is $G_r = 0$. Fourth, since the environment is supposed to be a flat and horizontal surface, the emitted energy from the environment in the direction of the surface of the object is $G_{env} = 0$. Fifth, energy E_r, reflected by the surface of the object (only the first reflection), is the sum of the reflected energy in the visible and the energy reflected in the infrared : $E_r = \rho(G_{dr} + G_{df}) + (1 - \epsilon)G_a$ where ρ is the reflectivity of the surface in the visible spectrum. The term $1 - \epsilon$ is the coefficient of reflection in the infrared according to Kirchhoff's law. Sixth, energy E_{rad} emitted by the surface of the object is governed by Planck's law: $E_{rad} = \epsilon\sigma T^4(0,t)$ where $T(0,t)$ is the temperature at the surface of the material ($x = 0$) at time t. Seventh, conducted energy E_{cd} within the material is given by $E_{cd} = -k\left(\frac{\partial T(x,t)}{\partial x}\right)_{x=0}$ Eighth, convective energy E_{cv} is $E_{cv} = h[T(0,t) - T_a(t)]$ where h is the convection coefficient. This coefficient is determined by using empirical formula [13] taking into account the wind speed V_a that is measured with an anemometer. Lastly, evaporation requires a certain amount of energy to transform water into water vapor. This energy is very often small with regard to other kinds of energy. However, this phenomenon cannot be neglected if materials are humid. In our modeling, we used an empirical formula, reasonably well adapted to our problem [8]: $E_{ev} = (a + bV_a)(P_s - P_v)$ where P_s is the pressure of saturating water vapor and P_v is its partial pressure. P_s and P_v depend on V_a, T_a that have been introduced previously and P_a (atmospheric pressure) that is also measured by a meteorological sensor.

2.3 Calculating Temperature of Objects

The equation of energy conservation is a boundary condition that describes the heat exchanges at the surface of bodies. Though necessary, this equation does not suffice to determine the temperature at the surface of the material. We also have to determine the temperature within the material. This is given by the well-known heat conduction equation which is a one-dimensional partial differential equation of the second order depending on time t and depth x in the material.

$$\frac{\partial T(x,t)}{\partial t} = a\frac{\partial^2 T(x,t)}{\partial x^2} \tag{3}$$

where $a = \frac{k}{\rho_m c_p}$ is the coefficient of diffusion of the material, k is the conductivity, ρ_m the density and c_p the specific heat. We need another boundary condition to describe how the temperature behaves on the other side of the material (i.e., for x higher than a certain depth). A reasonable assumption is that the temperature is constant for x higher than a critical dimension l that depends on the thermal parameters k, ρ_m and c_p:

$$\forall x \geq l, T(x,t) = T_l \tag{4}$$

Of course, this assumption requires that the depth of the object is at least equal to its critical dimension which is, in some cases, a severe limitation to our modeling.

Equations 2, 3 and 4 completely describe the thermal phenomena at the surface and within the material. Since some parameters such as $G_{dr} + G_{df}$, T_a and V_a are measured, it is necessary to rely on numerical analysis to calculate the temperature at the surface of the object. By using a finite difference method, it can be shown that these three equations can be written as follows:

$$\begin{cases} T_{m,n+1} = (1 - 2S)T_{m,n} + S(T_{m+1,n} + T_{m-1,n}) \\ H_n = C_1 {T_{0,n}}^4 + C_2 T_{0,n} + C_3 T_{1,n} \\ T_{m,n} = T_{m-1,n} \text{ si } m\delta x \geq l \end{cases} \tag{5}$$

where $S = \frac{1}{I^2}\frac{\delta t}{\delta y^2}$ (called stability coefficient that is a constant less than 0.5 to ensure convergence of the model), $H_n = (1 - \rho)(G_{dr,n} + G_{df,n}) + \epsilon(G_{a,n}) + hT_{a,n}$, $C_1 = \epsilon\sigma$,

$C_2 = h + \frac{1}{\delta y}$, $C_3 = -\frac{1}{\delta y}$, $\delta y = \frac{\delta x}{k}$, and δx and δt represent respectively the space step and the time step such that $x = m\delta x$ and $t = n\delta t$.

It is remarkable that the three physical parameters k, ρ_m and c_p are gathered within only one parameter $I = \sqrt{k\rho_m c_p}$ called thermal inertia. This is particularly interesting since it is now possible to reduce the class of possible materials to be studied from a three dimensional space (k,ρ_m,c_p) to a one-dimensional space I. This is done by setting $\delta y = \frac{\delta x}{k}$ that plays the same role as δx.

Knowing T_a, G_{dr}, G_{df} and V_a at each time step (measured by meteorological sensors) allows us to calculate the temperature at the surface of the body by solving System 5.

3 Recovering Physical Parameters

The resolution of System 5 allowed us to determine surface temperature for various values of ρ, ϵ and I such that $\rho = \frac{r}{31}$, $\epsilon = \frac{e}{31}$, $I = 4500 \times \frac{i}{31}$ where r, e and $i \in \{0, \cdots, 31\}$. The interval for I was chosen in order to contain solutions corresponding to materials of our experiment. $I = 0$ and $I = 4500$ respectively correspond to a material that does not conduct heat at all and a material that well conducts heat.

The basic idea of the method for recovering the three physical parameters of objects is to look for the vector $v = (\rho, \epsilon, I)$ among the set of possible combinations for which the modeled radiation best matches the experimental radiation measured by the camera. Mathematically, this can be done by minimizing the following least square fitting criterion:

$$\min_{v \in \{v_1, \ldots, v_{32768}\}} \frac{1}{N} \sum_{n=1}^{N} \frac{1}{\Delta_n^2} [G_{mod}(n) - G_{exp}(n)]^2 \qquad (6)$$

In Equation 6, N is the number of infrared images to be analyzed ($N = 360$, i.e, one image every four minutes). The term $G_{mod}(n)$ is the theoretical radiation received by the camera at time n. $G_{mod}(n) = E_{rad}(n) + E_{r_{ir}}(n) = \epsilon\sigma T_{mod}^4(n) + (1-\epsilon)G_a(n)$. The terms $G_{exp}(n)$ and Δ_n are respectively the mean experimental radiation received by the camera calculated in a squared patch of image n, M pixels in size, and the standard deviation of the radiation in the patch. Since we set ϵ to one in the electronics of the camera during our experiment, $G_{exp}(n) = \sigma T_{pseudo}^4(n)$ where $T_{pseudo}(n)$ is the temperature delivered by the camera in image n.

4 Experiment and Results

We have conducted a one day experimentation in outdoor scenes that consisted in acquiring infrared images of a sandbox ($3m \times 3m \times 0.7m$) filled with three kinds of sand. These dimensions allowed us to consider the sandbox to be a semi-infinite body. We also acquired meteorological parameters such as $G_{dr} + G_{df}$, T_a and V_a at the rate of one measurement every 6 minutes by using a meteorological station installed on the experimental site. The three layers of sand (gravel, medium sand and fine sand) $3m \times 1m$ in size can be seen in the visible in Figure 2 (a) and in the infrared in Figure 2 (b). These two images are not calibrated but are taken almost in the same direction. This allows us to have a good idea of how the three layers of sand appear in both images.

We applied the algorithm presented in Section 3 in order to calculate ρ, ϵ and I for the three kinds of sand. Figures 3 (a), (b) and (c) are intrinsic images of reflectivity, thermal inertia and emissivity of the sandbox (limited to the area of the three layers of materials). These images were obtained by applying the least-square fitting criteria to a sequence of $N = 360$ images. G_{mod} and G_{exp} were calculated in surface patches,

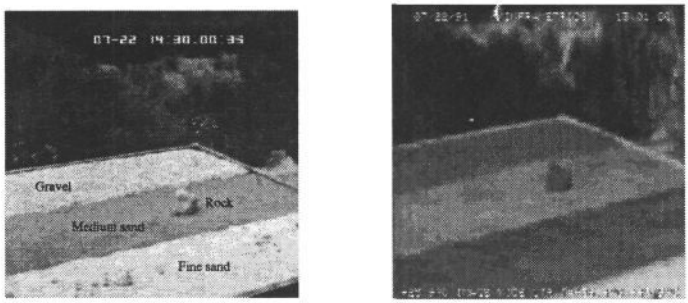

(a) Visible image (b) Infrared image

Figure 2: Visible and infrared images of the sandbox.

8 pixels in size. The calculation was repeated 64×64 different times in order to cover the entire image of 512×512 pixels. In fact, only the horizontal part of the sandbox can be correctly interpreted since our modeling assumes that the surface of objects is horizontal. At each point in the image, the grey level represents the physical parameters: reflectivity, thermal inertia or emissivity. White pixels correspond to points of the scene where the value of the physical parameter is high while dark pixels correspond to low values. Much information can be extracted from this set of three images that give a fairly good representation of actual physical parameters.

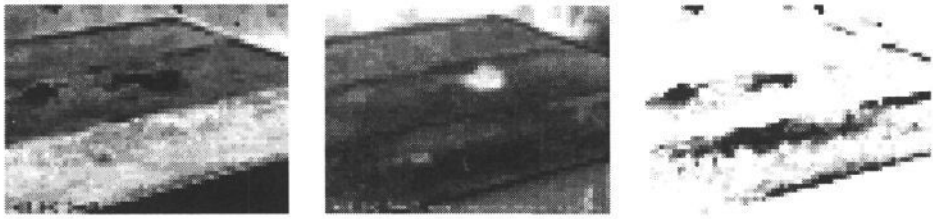

(a) Reflectivity (b) Thermal inertia (c) Emissivity

Figure 3: Intrinsic images of the sandbox.

Firstly, in Figure 3 (a), fine sand has a higher reflectivity than for gravel or medium sand. This is in accordance to actual data. A qualitative comparison with Figure 2 (a) shows that intensity levels are ordered the same for the three layers of sand. Points in the medium sand and gravel layers have similar intensity which means that they have close reflectivity. Again, this matches reality fairly well.

Secondly, in Figure 3 (b), the difference of thermal inertia between the three materials is small. However, one can notice that fine sand is slightly darker than medium sand, and

	ρ	ϵ	$I\ (Ws^{1/2}m^{-2}K^{-1})$
gravel modeled	0.56	1.0	565.0
actual	0.42	0.9	800.0 à 1000.0
medium modeled	0.53	0.99	377.0
actual	0.41	0.9	$\approx$500.0
fine modeled	0.64	0.96	284.0
actual	0.5	0.9	$\approx$300.0

Table 1: Modeled and actual characteristics of the three kinds of materials.

medium sand is darker than gravel. This is correct since the thermal inertia of fine sand is lower than the thermal inertia of medium sand, and the thermal inertia of medium is lower than the thermal inertia of gravel. Furthermore, though the small rock does not satisfy the assumption of semi-infinite body (surface not horizontal), it appears whiter than the three other materials which means that its thermal inertia is higher than for the three other materials. This matches actual data. In Figure 3 (b), a small white patch in the left part of the fine sand layer was correctly displayed and corresponds to a pebble that is almost not perceptible in Figure 2 (a).

Lastly, Figure 3 (c) is composed of white areas where emissivity is equal to one and black areas where emissivity is close to 0.7. This shows that this parameter globally takes high values. However, emissivity can be somewhat different from point to point in the image. In fact, high variations of the emissivity cause relatively small variations in temperature. Therefore, small errors in temperature measurements can cause high variations in the emissivity.

Quantitative results are presented in Table 1. For each material, modeled values were determined by applying our algorithm to one given patch of surface. All modeled values for ρ and ϵ are higher than actual ones while modeled values for I are lower than actual ones. We think that there are two types of explanation for these errors; on one hand, approximated modeling for atmospheric radiation, convective radiation and evaporation, on the other hand, errors due to the non-linearity for the conduction equation.

The first kind of errors are called systematic errors and their treatment is often awkward because they are closely related to measurement errors [9]. The second kind of errors is due to stability of the backward process. In the following, we will concentrate on the second kind of errors because they are intrinsic to the inverse process.

5 Inverse Problem Analysis

For numerous applied problems, it is important to analyze the stability of solutions with regard to small variations of initial data (i.e., physical parameters). Problems that do not satisfy this condition of stability are said "ill-posed" [10]. To solve these problems, one has to define the concept of approximate solutions. In our case, the temperature of objects depends on a vector v of physical parameters $v = (\rho, \epsilon, I)$. Let us call A_T the application $\mathcal{V} \stackrel{A_T}{\rightarrow} \mathcal{T}$ that associates at each vector v in space $\mathcal{V}$ the curve of temperature of the material in space $\mathcal{T}$ (on a period of time $2\pi/\omega = 24hours$). One may define a distance $d(T_1, T_2)$ between two curves of temperature T_1 and T_2 in space $\mathcal{T}$:

$$d(T_1, T_2) = \frac{\omega}{2\pi} \{ \int_{t_1}^{t_2} [T_2(t) - T_1(t)]^2 dt \}^{1/2} \tag{7}$$

Let us now define a distance $d(v_1, v_2)$ between two vectors of physical parameters in space $\mathcal{V}$ where $T_1 = A_T(v_1)$ and $T_2 = A_T(v_2)$; $d(v_1, v_2) = \sqrt{(\rho_2 - \rho_1)^2 + (\epsilon_2 - \epsilon_1)^2 + (I_2 - I_1)^2}$.

To analyze the inverse problem, two questions have to be studied:

- Unicity of the solution of the inverse problem?
- Stability or sensitivity to noise?

In order to discuss the first question, it is convenient to have an analytical solution for the direct problem (i.e., an analytical expression of the temperature at the surface of the object as a function of physical parameters). We obtained such an equation in [2] under the following assumptions. First, the surface of the object is planar and horizontal. Second, solar radiation is modeled as a semi-sinusoidal function of time (no radiation at night). Third, the atmosphere temperature is approximated by a sinusoidal function whose period is equal to 24 hours with its maximum during sunshine and its minimum at night. Fourth, wind speed is modeled by its mean value on a one day interval. Fifth, because of the rather small dynamics of material temperature (compared yo its mean value), the infrared radiation emitted by the surface that is the fourth power of the temperature is modeled as a linear function: $\sigma T^4 \approx A + BT$ where $A = -945$ and $B = 4.62$.

The calculation that leads to the complete analytical expression of the temperature is rather complicated and we have not enough space to report it here (see [2] for details). This temperature is a function of numerous parameters: reflectivity of the surface ρ, emissivity of the surface ϵ, thermal inertia of the material I, solar constant, solar declination, latitude, emissivity of the atmosphere ϵ_a, transmissivity of the atmosphere, temperature of the atmosphere T_a and wind speed V_a. If we suppose that $\epsilon_a = 1$ and the amplitude of the atmosphere temperature is zero, then this expression leads to a simpler equation that can be written as a function of time t and two parameters called λ_1 and λ_2:

$$T(t, \lambda_1, \lambda_2) = C_0 + C_1\lambda_2 + \frac{C_2\lambda_2}{\sqrt{1 + 2a_0\lambda_1 + 2{a_0}^2\lambda_1^2}} \cos(\omega t - \theta(\lambda_1)) + \\ + \sum_{n=2}^{\infty} \frac{C_3(n)\lambda_2}{\sqrt{1 + 2a_0 n^{1/2}\lambda_1 + 2{a_0}^2 n\lambda_1^2}} \cos(n\omega t - \theta_n(\lambda_1)) \qquad (8)$$

where C_0 is a constant. C_1, C_2 and $C_3(n)$ depend only on latitude and solar declination and,

$$\lambda_1 = \frac{I}{\epsilon B + h} \qquad (9)$$

$$\lambda_2 = \frac{1 - \rho}{\epsilon B + h} \qquad (10)$$

Equation 8 depends only on λ_1 and λ_2 and not on ρ, ϵ and I separately. The assumptions that lead to this result are quite realistic since ϵ_a is in many cases close to one and the amplitude of the atmosphere temperature is much lower than the amplitude of surface temperature.

Equation 8 is an important result since it means that two materials with different physical parameters but with same λ_1 and λ_2 will have the same thermal behavior at their surface and are therefore not distinguishable. We will call these parameters **"physical invariants"** because objects with the same λ_1 and the same λ_2 will have the same temperature. Therefore, λ_1 and λ_2 describe distinguishable class of solutions of the inverse process for the heat conduction problem and can be used to distinguish between two different class of materials. Since λ_1 and λ_2 are physical invariants, $\lambda_3 = \frac{\lambda_1}{\lambda_2} = \frac{I}{1-\rho}$ is

also an invariant that has the pecularity to be solely dependent on the physical parameters of the material.

Figure 4 shows the geometrical representation of λ_1 and λ_2 in the $3D$ space of the physical parameters ϵ, ρ and I. Figure 4 (a) represents physical parameters that are solutions of Equations 9 and 10 where λ_1 and λ_2 have constant values. The intersection line of the two planes is the solution of $T(t, \epsilon, \rho, I) = T(t, 0.9, 0.5, 500) = T(t)$. Therefore, the solution to backsolving the heat conduction equation is not unique. This non-unicity can be explained in terms of physical invariants that give rise to class of possible solutions.

In order to analyze noise effect, we used our numerical modeling to calculate the temperature $T(t)$ of a material that has the same physical parameters as previously: $\epsilon = 0.9$, $\rho = 0.5$ and $I = 500 W s^{1/2} m^{-2} K^{-1}$. A gaussian noise with mean value equal to zero and standard deviation $\sigma = 0.8$ was added to this temperature. In Figure 4 (b), the two point sets respectively correspond to the best solutions $T_2(t)$ for $d(T_1, T_2) < 0.2$ where $d(T_1, T_2)$ is defined by Equation 7 with $T_1(t) = T(t, 0.9, 0.5, 500)$ and $T_1(t) = T(t, 0.9, 0.5, 500) + \sigma$. A threshold of 0.2 was chosen because the noise equivalent temperature difference that can be perceived by the infrared camera of our experiment is equal to $0.2°C$. In Figure 4 (c), the two line segments are least square approximations of the two point sets of Figure 4 (b). These two line segments are almost superposed which means that the solutions of physical parameters found by Equation 7 are little dependent on noise. As obtained with the analytical model, the solutions given by the numerical model is a line segment in the 3D space of the physical parameters showing the non-unicity of the solution.

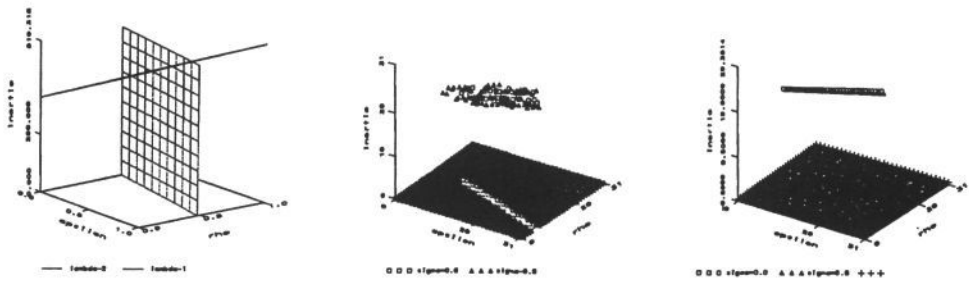

(a) Theoretical data (b) Experimental data (c) Linear approximations

Figure 4: Solutions to the inverse problem for the heat equation. In (a), $I \in [0, 519]$, ϵ and $\rho \in [0, 1]$. In (b) and (c), $I \in [100, 600]$, $\epsilon \in [0.7, 1.0]$ and $\rho \in [0.4, 0.7]$.

6 Conclusion

For many years, researchers working on early vision problems have been interested in recovering physical properties of objects such as reflectivity and shape from classical images. In this article, we addressed the problem of determining physical parameters of objects such as reflectivity, emissivity and thermal inertia in infrared images.

We developed a complete numerical modeling based on physical laws of heat transfer in order to understand how points of semi-infinite objects, whose surface is planar and horizontal, appear in infrared images. Then, we presented a method for recovering the three physical parameters of objects. Applying this method to an outdoor scene composed of three kinds of sand lead to reasonable results. In particular, fairly good intrinsic images of physical parameters were obtained. However, the analysis of an analytical expression of the temperature allowed us to show that the vector of physical parameters is not unique. We found the existence of physical invariants that describe this non-uniqueness; objects that have different physical parameters but have the same invariants are not distinguishable. On the contrary, class of objects that have different physical invariants can be distinguished. Physical invariants are therefore more reliable than physical parameters to discriminate objects.

7 Acknowledgments

The author would like to thank T. Porcher for his assistance in implementing the model.

References

[1] M. Bertero, T. Poggio, and V. Torre. Ill-Posed Problems in Early Vision. *IEEE Special Issue on Computer Vision*, 76(8):869–889, August 1988.

[2] C. Caillas. Thermal Imaging for Robotic Applications in Outdoor Scenes. Technical Report CMU-RI-TR-90-08, The Robotics Institute, Carnegie Mellon University, 1990.

[3] B. K. P. Horn. Understanding image intensities. *Artificial Intelligence*, 8(2), 1977.

[4] S. B. Idso and R. D. Jackson. Thermal radiation. *Geophysical Research*, 82(28), September 1977.

[5] T. Kanade and K. Ikeuchi. Introduction to the Special Issue on Physical Modeling in Computer Vision. *IEEE Trans. Pattern Anal. Machine Intell.*, 13(7):609–610, July 1991.

[6] G. J. Klinker, S. A. Shafer, and T. Kanade. A Physical Approach to Color Image Understanding. *International Journal of Computer Vision*, 4(1):7–38, 1990.

[7] S. K. Nayar, K. Ikeuchi, and T. Kanade. Surface Reflection: Physical and Geometrical Perspectives. *IEEE Trans. Pattern Anal. Machine Intell.*, 13(7):611–634, July 1991.

[8] R. A. Roy, editor. *Databook of Heat Transfer and Fluid Flow.* Genium Publishing Corporation, Schenectady, New York.

[9] J. R. Taylor. *An Introduction to Error Analysis. The Study of Uncertainties in Physical Measurements.* University Science Books, 1982.

[10] A. N. Tikhonov and V. Y. Arsenin. *Solutions of Ill-Posed Problems.* Washington, DC: Winston & Sons, 1977.

[11] F. M. White. *Heat and Mass Transfer.* Addison Wesley, 1988.

[12] R. J. Woodham. Reflectance map techniques for analyzing surface defects in metal castings. Technical Report AI-TR-457, Mass. Inst. Technol., Artificial Intell. Lab., Cambridge. MA, 1978.

[13] G. J. Zissis and W. L. Wolfe. *The Infrared Handbook.* Office of Naval Research, Department of the Navy, Washington, DC, 1978.